Radiation Measurements 82 (2015) 64–73

Contents lists available at ScienceDirect

Radiation Measurements

journal homepage: www.elsevier.com/locate/radmeas

EURADOS ^{241}Am skull measurement intercomparison

P. Nogueira [a, b, *], W. Rühm [a], M.A. Lopez [c], T. Vrba [d], W. Buchholz [e], P. Fojtík [f], G. Etherington [g], D. Broggio [h], J. Huikari [i], O. Marzocchi [j, 1], T. Lynch [k], A.L. Lebacq [l], C. Li [m], J. Ośko [n], I. Malátova [f], D. Franck [h], B. Breustedt [o], D. Leone [o], J. Scott [g], A. Shutt [g], B. Hauck [m], K. Capello [m], B. Pérez-López [c], J.F. Navarro-Amaro [c], T. Pliszczyński [n], K. Fantínová [f], S.Y. Tolmachev [p]

[a] Helmholtz Zentrum München, National Research Center for Environmental Health, Institute of Radiation Protection, Ingolstädter Landstr. 1, 85764 Neuherberg, Germany
[b] Thünen Institute of Fisheries Ecology, Marckmannstraße 129b, 20539 Hamburg, Germany
[c] CIEMAT, Centro de Investigaciones Energéticas Medioambientales y Tecnologicas, Avda Complutense 40, 28040 Madrid, Spain
[d] Czech Technical University in Prague, Brehova 7, 11519 Prague, Czech Republic
[e] BfS, Federal Office for Radiation Protection, Department of Radiation Protection and Health, 85764 Oberschleißheim, Germany
[f] NRPI, National Radiation Protection Institute, Prague, Czech Republic
[g] PHE, Public Health England, CRCE, Didcot OX11 0RQ, United Kingdom
[h] IRSN, Radiological Protection and Human Health Division, BP17, 92262 Fontenay-aux-Roses Cedex, France
[i] STUK, Radiation and Nuclear Safety Authority Radiation and Nuclear Safety Authority, Finland
[j] KIT, Karlsruhe Institute of Technology, Hermann-von-Helmholtz-Platz 1, 76344 Eggentein-Leopoldshafen, Germany
[k] Mission Support Alliance, Richland, WA, USA
[l] SCK•CEN, Studiecentrum voor Kernenergie (Belgian Nuclear Research Centre), Mol, Belgium
[m] HML, Health Canada, Human Monitoring Laboratory/Radiation Protection Bureau, Ottawa, Ontario, Canada
[n] NCBJ, National Centre for Nuclear Research, A. Soltana 7, 05-400 Otwock, Poland
[o] Institute for Nuclear Waste Disposal, Karlsruhe Institute of Technology, Hermann-von-Helmholtz-Platz 1, 76344 Eggentein-Leopoldshafen, Germany
[p] United States Transuranium and Uranium Registries, College of Pharmacy, Washington State University, 1845 Terminal Drive, Suite 201, Richland, WA 99354, USA

HIGHLIGHTS

- The results revealed some of the difficulties associated with the phantoms use.
- The results obtained show that it is necessary the fabrication of a new phantom.
- The participants validated their measurements and calibrations.
- This work contributed for the harmonization of skull measurements and calibration.

ARTICLE INFO

Article history:
Received 13 March 2015
Received in revised form
24 June 2015
Accepted 30 July 2015
Available online 3 August 2015

Keywords:
EURADOS
Intercomparison
Skull phantom
Americium-241
Partial body counter
In vivo

ABSTRACT

In 2011 a measurement intercomparison was launched by EURADOS WG7, with the objective of providing the participants with the tools to calibrate their detection systems for detection of ^{241}Am in the skull bone, and evaluate the variability due to the used of the different calibration phantoms. Three skull phantoms were used in this intercomparison: the USTUR Case 0102 skull phantom, the BfS skull phantom and the CSR skull phantom. Very good agreement was found between the results of the twelve participating laboratories, with relative deviations of less than 15% for the BfS phantom and less than 17% for the USTUR phantom when measurement efficiency in defined positions was compared. However, the phantoms' measured absolute ^{241}Am activities showed discrepancies of up to a factor of 3.4. This is mainly due to the physical differences between the standard calibration phantoms used by the participants and those used in this intercomparison exercise.

* Corresponding author. Helmholtz Zentrum München, National Research Center for Environmental Health, Institute of Radiation Protection, Ingolstädter Landstr. 1, 85764 Neuherberg, Germany.
E-mail address: pedro.nogueira@ti.bund.de (P. Nogueira).
[1] European Patent Office, Patentlaan 2, 2288EE Rijswijk, Netherlands.

http://dx.doi.org/10.1016/j.radmeas.2015.07.011
1350-4487/

1. Introduction

"Bone-seeking" radionuclides are of special concern since on the long term they are incorporated into the bone matrix. More specifically, according to their biokinetics, these radionuclides could be divided in two categories, i.e., the "bone-volume seekers" and "bone-surface seekers". ^{241}Am belongs to the latter one and, as other "bone-surface seeking" radionuclides which deposits on bone surfaces and thus irradiate osteocytes and also red bone marrow and because of its long physical (432.6 years) and biological half – life (46.6 years in the skeleton according model from ICRP-78 (1997), it has a high radiotoxicity It could be found in the environment following nuclear reprocessing, nuclear weapons test in atmosphere and major nuclear accidents. Moreover, it can be found in daily life objects such as smoke detectors.

^{241}Am can be detected and assessed by *in vivo* gamma monitoring of the lungs and/or the skeleton, usually through the 59.54 keV photons emitted with a high yield of 35.92% (Ferreux, 2008). Due to the low energy of these photons, detectors are usually arranged around and close to the surface of a certain body region, to increase the counting efficiency of the detection system. This procedure is called Partial Body Counting (PBC). Typical sites of the human body used are the lungs, the skull and the knees. The two latter counting regions are convenient due to the overlying thin soft tissue that absorbs a smaller fraction of the emitted low-energy photons compared to the thicker soft tissue covering the lung region, thus allowing for a higher detection efficiency.

PBC detection systems require efficiency calibration with anthropomorphic phantoms, which reproduce the shape and attenuation characteristics of the measured region of the human body and contain a known activity of the radionuclide of interest. For knee measurements, there are a number of commercial knee phantoms available, such as the Spitz knee phantom (Spitz and Lodwick, 2000). Such commercial phantoms for skull geometries do not exist. Currently, there are only a limited number of dedicated non-commercial skull phantoms available worldwide. Due to the uniqueness of each of these phantoms and due to the lack of a standardized manufacturing process, the calibration process of PBC detection systems and the activity estimation performed in different laboratories include large uncertainties. As it was observed by Rühm et al. (1998) the use of different skull phantoms for calibration resulted in differences of up to 60% between assessments in different laboratories.

The European Radiation Dosimetry Group (EURADOS) Working Group 7 (WG7) is acting as a network in the field of Internal Dosimetry for scientists, services, regulators, and laboratories whose main aims are harmonization, coordination of research, training, and dissemination of scientific knowledge in the field of the assessments of internal exposures due to intakes of radionuclides (Lopez et al., 2011; Lopez and Nogueira, 2012).

In 2011, a skull measurement intercomparison was launched by EURADOS WG7, with the objective of providing the participants with the tools to calibrate their detection system for skull counting geometries. The protocol of the exercise was designed to allow for the assessment of the measurement reproducibility of different laboratories. This required assessment of the ^{241}Am activity of different phantoms, to determine the capabilities of the PBC systems available in the frame of the EURADOS network. Parallel to this action a Monte Carlo exercise was launched, to evaluate and to promote the use of Monte Carlo methods for calibration of PBC systems.

There were 12 participants in this intercomparison: 10 from Europe – Helmholtz Centre Munich (HMGU, Germany), Federal Office for Radiation Protection (BfS, Germany), Karlsruhe Institute of Technology (KIT, Germany), National Radiation Protection Institute (NRPI, Czech Republic), Slovak Medical University (SZU, Slovakia), Belgian Nuclear Research Centre (SCK·CEN, Belgium), Institute for Radiological Protection and Nuclear Safety (IRSN, France), Centre for Energy, Environment and Technology Investigations (CIEMAT, Spain), Public Health England (PHE, UK), Finnish Radiation and Nuclear Safety Authority (STUK, Finland), National Centre for Nuclear Research (NCBJ, Poland); two from North America – the Mission Support Alliance (MSA, USA), and Health Canada (HC, Canada).

Three skull phantoms, were used in this intercomparison: the USTUR Case 0102 skull phantom, the BfS phantom and the CSR hemispherical phantom. From the initial fourteen participants, finally a total of twelve laboratories from Europe and North America delivered results. These results are presented and discussed in detail in this paper.

2. Methods

The intercomparison exercise was divided in two tasks. Task one included measurement at predefined positions on the surface of the skull phantoms, at 1 cm distance. The second task required estimation of the absolute ^{241}Am activities of the three phantoms used. This task was for participants who had already calibrated their PBC system previously with another physical skull phantom or who are using Monte Carlo methods to calibrate their systems. Several of the participants also participated in the EURADOS Monte Carlo skull phantom intercomparison (Vrba et al., 2015, 2014b). To be consistent, the same participant ID was used here, for those who participated in both intercomparisons.

In order to estimate the accuracy of the results, the Gaussian propagation of the counting statistic, emission probability, and the phantoms activities was performed using the values presented in Table 1 for a confidence level of approximately 68% ($k = 1$).

3. Detection systems

Despite the fact that most of the detectors used by the participants were commercial germanium crystals built by only two companies, all PBC systems were quite different in terms of the number of detectors, crystal dimension, end-cap window, flexibility in geometry, and dedicated shielding (see Fig. 1 and Table 2).

In Table 3 one can find details on the intercomparison measurements times, PBC detectors energy calibration, energy range typically used by the participant in routine measurements and software used for the spectrum analysis. Concerning the laboratories natural radioactive background, most participants have subtracted this contribution to the count rate, by determining the counts on the left and on the right of the ^{241}Am 59.54 keV peak to calculate the number of counts under this peak (the background counts). The number of background counts was then subtracted from the total number of counts in the 59.54 keV peak area. Only a few participants have previous to this step, monitored the natural background and subtracted the measured radionuclides peak areas

Table 1
Uncertainty values for a confidence level of 95% ($k = 2$) used for the efficiency uncertainty and normalization results uncertainty.* Note that the counting statistic value and uncertainty depends on each of participant measurement.

Source of uncertainty	Value	Uncertainty ($k = 2$)
Counting statistic	–	>2%*
Emission probability	0.3592	0.0034
USTUR phantom activity	287.2	7.4
BfS phantom activity	5239.3	226.8
CSR phantom activity	981.4	19.6

from the phantom measurement spectrum. Since the ^{241}Am is not one of the typical background radionuclides in a PBC laboratory background, no difference between both the approaches is expected.

4. Phantoms and measurement positions

For task 1 all the measurements were performed at a distance of 1 cm between the phantom surface and the detector. For this purpose, a Plexiglas (polymethyl methacrylate) plate was provided to the participants together with the phantoms, to be used as a spacer between the phantom and the detector surface. Each participant freely chose the count time of the measurement; however, it was recommended that the relative counting uncertainty of the 59.54 keV net peak area should be below 1% ($k = 1$).

Results of measurements performed by the first author of this paper (PN) before the intercomparison exercise commenced were presented in 2011 at the EURADOS WG7 meeting at Gent, Belgium. These results showed that the inclination between the detector and the phantom surface, could affect the detection efficiency. Thus, the inclinations used by the HMGU detector were advised to be also used by the participants (see Table 4 and Table 5).

4.1. USTUR case 0102 skull phantom

The Case 0102 is the first whole-body donation to the United States Transuranium and Uranium Registries' (USTUR) (Table 6). This individual was accidentally exposed to ^{241}Am about 25 years prior to his death (Breitenstein et al., 1985). The skeleton divided postmortem along the sagittal plane. The left side of the skeleton was radiochemically analyzed (McInroy et al., 1985) while the right side was used to build anthropomorphic phantoms from skull, torso, arm and leg for *in vivo* counting systems (Hickman and Cohen, 1988). The USTUR phantoms are unique since they contain a real human skeleton with a natural metabolic ^{241}Am activity incorporation into the bone matrix.

The USTUR Case 0102 skull phantom consists of one-half (bilateral slice) with ^{241}Am contaminated bones from the exposed individual on the right side, and non-contaminated bones on the left side. The phantom is filled and covered with tissue equivalent material (Hickman and Cohen, 1988). A recent re-evaluation of the activity content indicates that this skull phantom contains 287.2 ± 3.7 Bq of ^{241}Am at the reference date January 1, 2012 (Tolmachev, 2012).

4.2. USTUR skull phantom measurement geometry

For the measurement of the USTUR skull phantom, five positions were defined over the sagittal cut of the phantom, and on the side that contains active bones; however, positions 3 and 4 were optional (see Fig. 2). Additional optional positions, −2 and −3, were proposed for participants who desired to estimate the cross counting (additional counting rate obtained on the measurements at positions 2 and 3 if the non-contaminated bone were contaminated). These positions were proposed based on the fact that the majority of *in vivo* laboratories use a symmetrical measurement geometry with an even number of detectors (Vrba, 2010), and on results obtained from an extensive set of measurements performed by HMGU before the EURADOS intercomparison using a collimated detector, with the aim to determine the positions on the skull phantom that provide the highest detector counting rates.

4.3. BfS phantom

The BfS skull phantom contains a human bone artificially labelled with ^{241}Am. It was fabricated by the New York Medical Center, USA, for the Federal Office of Radiation Protection (BfS, Germany).

The interior of the phantom is filled with small spheroids of paraffin wax, while the outside is covered with a layer of the same material with a constant thickness (of 6 mm) that corresponds to the average thickness of soft tissue covering the human skull of an average person. The ^{241}Am activity was artificially put on the bone surfaces as follows: small rectangular pieces of absorbent filter paper were impregnated, via calibrated syringe, with a known amount of ^{241}Am solution. These activated filter papers were distributed along the bone surface as follows: 3000 Bq on the outside bone surface and 2400 in the inner bone surface, resulting in a total activity of 5400 ± 113.4 Bq at the reference date March 1, 1993 (Laurer, 1993).

4.4. BfS phantom measurement geometry

Five positions were defined and marked on the BfS phantom based on the results obtained from a previous international intercomparison (Rühm et al., 1998) using this phantom (see Fig. 4).

4.5. CSR phantom

The CSR phantom is a completely artificial phantom that was produced to represent the top of a human head. It is the product of collaboration between the National Radiation Protection Institute (NRPI, Czech Republic) and the Slovak Medical University Bratislava (SZU, Slovak Republic) (Vrba et al., 2014a). This phantom not design for the calibration of PBC but was specifically developed for this intercomparison, in order to provide a link between the measurement results and the Monte Carlo simulation results, by taking advantage of its simple geometry and defined material composition.

The phantom consists of three parts: a bone tissue substitute that is made of gauze and a plaster of Paris modelled into a hemispherical cap; and two soft tissue substitutes cast from GAFORM E45 that substitute the brain by filling the inner space of the cap, and the scalp tissue by covering the outer surface with a thickness of 8 mm−11 mm of GAFORM E45.

The phantom contains 981.4 ± 9.8 Bq of ^{241}Am at the reference

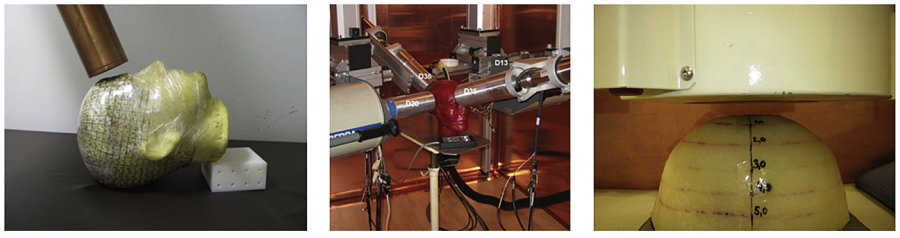

Fig. 1. Three of the partial body counter systems that were used in the EURADOS intercomparison belonging to SCK•CEN, NRPI, and IRSN (from left to right).

Table 2
Details of partial body counters used by the participants in this intercomparison; information given is based on manufacture data sheets. To preserve anonymity, only the participant numbers are given.

Participant number	Detector			Germanium crystal			Window	
	Number	Type	Manufacturer	Active area (mm^2)	Diameter (mm)	Length (mm)	Material	Thickness (mm)
P01	3	BEGe	Canberra	4418	75	20	Carbon fiber	Unknown
P02	4	GEM	Ortec	5675	85	30	Carbon fiber	0.76
P03	2	LEGE	Canberra	2922	61	20	Carbon fiber	0.5
P04	4	LO-AX	Ortec	3848	70	30	Carbon fiber	0.76
		LO-AX	Ortec	3848	70	30	Beryllium	0.5
		BEGe	Canberra	3848	70	25	Carbon fiber	0.6
		GEM-FX	Ortec	3848	70	27.6	Carbon fiber	0.9
P07	4	XtRa	Canberra	4418	75	72	Carbon fiber	0.5
P09	2	HPGe	Canberra	3848	70	20	Carbon fiber	0.6
				3848	70	30	Carbon fiber	0.6
P11	2	BEGe	Canberra	5027	80	30	Carbon fiber	1.6
P12	4	GEM-FX	Ortec	3848	70	25	Carbon fiber	0.76
P14	4	EGM2000	Eurisys Canberra	1963	50	10	Carbon fiber	1.1
		EGM2000	Eurisys Canberra	1963	50	10	Carbon fiber	1.1
		Be5020	Canberra	5153	81	22	Carbon fiber	0.5
		LOAX	EG&G Ortec	3926	70.7	29.5	Carbon fiber	0.76
P15	4	LEGe	Canberra	3848	70	25	Carbon fiber	0.5
P18	1	GX-4018	Canberra Packard	2827	60	66	Aluminium	1.5
P23	4	HPGe	Canberra	2003	50.5	20	Carbon fiber	0.5

Table 3
Details on the measurement times for each phantom, radionuclides used for the energy calibration of the detector, energy range of typical measurements and spectrum analysis software used by the participants in this intercomparison. To preserve anonymity, only the participant numbers are given.

Participant number	Measurement time (s)			Energy calibration	Used typically in the energy range (keV)	Spectrum analysis software
	USTUR	BfS	CSR			
P01	9000	1000	4600	2 point sources:^{241}Am and ^{60}Co	20–2000	Home made program
P02	60000	60000	60000	mixed^{152}Eu and ^{241}Am standard	10–500	Ortec Renaissance v4.01
P03	60000	1000	2000	2 point sources:^{241}Am and ^{133}Ba	25–400	Genie 2000 v3.2.1
P04	100000	5000	2000	4 point sources:^{241}Am, ^{210}Pb, ^{57}Co and ^{137}Cs	14–200	Genie 2000 v3.2
P07	7200	900	1800	3 point sources:^{241}Am, ^{137}Cs and ^{60}Co	40–200	Genie 2000 v3.2
P09	7200	3000	3000	2 point sources:^{241}Am and ^{152}Eu	17–200	Abacos Plus v5.3
P11	68400	86774	31308	4 point sources:^{241}Am, ^{133}Ba, ^{137}Cs and ^{60}Co	13–2000	Genie 2000 v3.1a
P12	50000	2000	15000	2 point sources:^{241}Am and ^{152}Eu	15–1000	Genie 2000 v3.2.1
P14	7200	2000	4000	2 point sources:^{241}Am and ^{152}Eu	20–200	Gamma Vision v5.33
P15	10800	1800	7200	2 point sources:^{241}Am and ^{152}Eu	10–1000	Abacos 2000/Genie2000 v1.2
P18	200427	78760	86400	3 point sources:^{241}Am, ^{137}Cs and ^{60}Co	40–2000	Genie 2000 v3.1a
P23	10800	1200	1800	4 Point sources:^{241}Am, ^{57}Co, ^{137}Cs and ^{60}Co	15–1750	LVis v2.1.0.5

date January 1, 2012, that was implanted in the bone substitute in the form of drops, distributed in 418 nodes of a reference grid, 228 drops on the outside surface and 192 drops on the inside.

4.6. CSR phantom measurement geometry

Only one position was defined for the CSR phantom measurement, due to the simple geometry and shape of this phantom: the detector should be placed 10 mm above the top of the phantom as shown in Fig. 5.

Independently of the phantom used, the detection efficiency was calculated by dividing the net area of the 59.54 keV peak by the phantom activity, emission yield and the measurement time. The corresponding one-sigma uncertainty was calculated through Gaussian propagation of the counting uncertainty, the gamma emission yield uncertainty and the phantom activity uncertainty.

5. Results

5.1. Task 1 measurements of intercomparison positions

The results obtained by the participants for the detection efficiency at 59.54 keV were plotted as a function of the detector

Table 4
Measurement positions and inclination angles between detector and the surface of USTUR Case 0102 skull phantom recommended to be used by the participants. For reference orientation system see Fig. 3. For all positions the detector endcap-window was at 10 mm distance from the phantom surface.

Position	Inclination (degrees)
0	90°
1	34.5°
2 and −2	0°
3 and −3	−16.8°
4	26.5°

Table 5
Measurements positions and inclination angles between detector and the surface of the BfS phantom recommended to be used by the participants. Orientation system according to Fig. 3.

Position	Inclination (degrees)
1	43°
3	57°
4	0°
7	0°
12	0°

Table 6
Task 1 detection efficiencies obtained for the USTUR phantom. NP – not provided by the participant. The uncertainty values correspond to the Gaussian uncertainty propagation of the net peak area uncertainty, the gamma emission yield uncertainty and the phantom activity uncertainty.

Position	Participant efficiency and uncertainty (10^{-3}cps/Bq)					
	P01	P02	P03	P04	P07	P09
0	9.31 ± 0.16	12.7 ± 0.49	7.57 ± 0.13	10.10 ± 0.21	11.20 ± 0.24	8.87 ± 0.16
1	7.75 ± 0.14	8.96 ± 0.13	5.15 ± 0.10	8.50 ± 0.17	8.09 ± 0.20	7.52 ± 0.14
2	10.9 ± 0.18	15.5 ± 0.22	8.34 ± 0.15	11.9 ± 0.22	13.20 ± 0.28	12.30 ± 0.24
3	11.3 ± 0.18	NP	8.10 ± 0.14	NP	11.90 ± 0.26	10.90 ± 0.19
4	6.98 ± 0.14	8.51 ± 0.12	5.16 ± 0.10	7.23 ± 0.15	7.40 ± 0.19	NP
	P11	P12	P14	P15	P18	P23
0	14.00 ± 0.23	9.19 ± 0.13	6.27 ± 0.13	10 ± 0.28	2.86 ± 0.05	5.53 ± 0.11
1	9.19 ± 0.13	6.28 ± 0.10	4.10 ± 0.09	7.07 ± 0.25	2.39 ± 0.04	3.68 ± 0.09
2	15.90 ± 0.22	10.5 ± 0.18	6.58 ± 0.13	11.60 ± 0.32	3.35 ± 0.05	6.24 ± 0.12
3	NP	9.55 ± 0.14	6.32 ± 0.12	11.20 ± 0.24	3.09 ± 0.05	6.22 ± 0.13
4	NP	6.02 ± 0.09	4.11 ± 0.09	6.60 ± 0.18	2.21 ± 0.04	3.69 ± 0.09

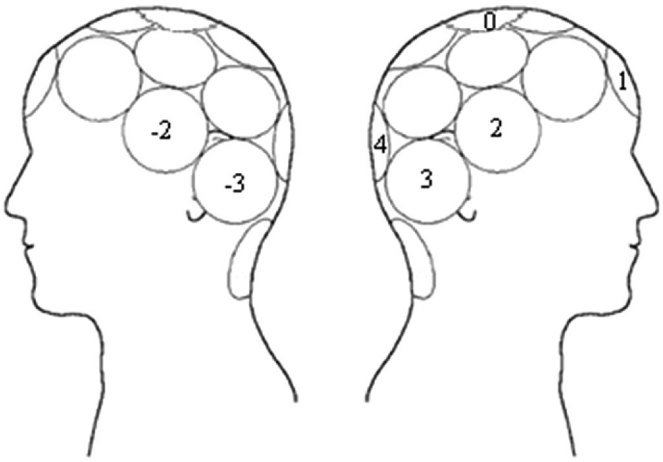

Fig. 2. Measurements positions (−2, −3, 0, 1, 2, 3, 4) defined on the USTUR skull phantom on the right and left side. Figure adapted from Rühm et al. (1998).

diameter, and regression lines were fitted between the measurement positions. In Fig. 6, the regression lines obtained for the USTUR skull phantom show that – as expected – the detection efficiency is proportional to the detector diameter. Note, however, that there are some exceptions for detectors which show different efficiencies although they have the same diameter. Also, the P18 efficiency is significantly lower than that of the other participants, at a detector diameter of 60 mm. Fig. 6 also shows a significant variation of the detection efficiency with measurement position. The reason for this is that a) only half of the skull bone is active in this phantom, b) a different thickness of the soft tissue material is used at different positions, and c) the ^{241}Am activity distribution pattern present in the USTUR skull phantom is inhomogeneous (Hickman and Cohen, 1988).

The results obtained for the CSR phantom were also plotted as a function of the detector diameter. In Fig. 8 one can see that – as expected – the detector efficiency increases with the crystal diameter of the detector. Monte Carlo simulations performed by one of the co-authors (TV) and presented at the EURADOS annual meeting in Barcelona, Spain, in 2014, demonstrated that detection efficiency increases according to a power function of the diameter, for identically constructed detectors with different crystal diameter. In the present work, however, it was not possible to observe such a pattern, due to differences in detector materials, distance between the endcap window and the crystal, and crystal dead layer thickness characteristic for the detectors of the participants. As a result of these intrinsic differences, detectors with the same crystal diameter have different efficiencies.

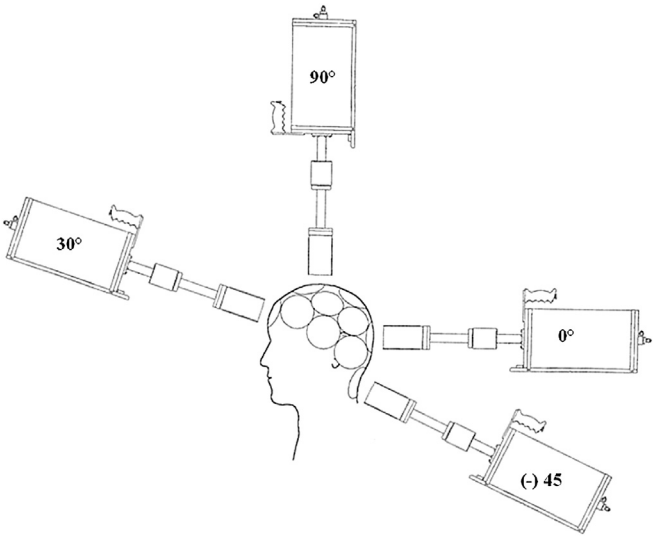

Fig. 3. Examples of measurement inclination angles between detector and the surface of the phantoms to be used by the participants.

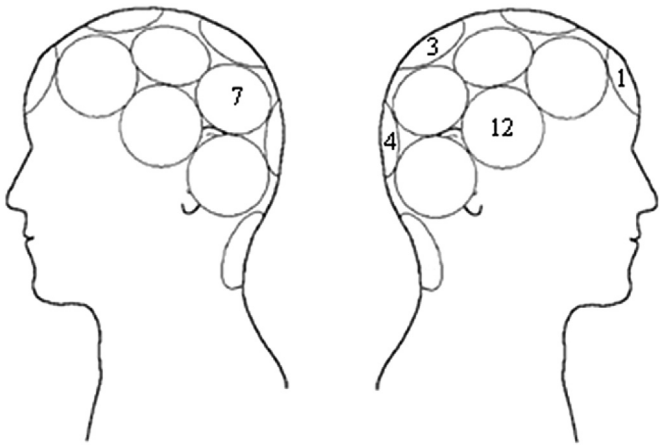

Fig. 4. Measurement positions (1, 3, 4, 7 and 12) defined on BfS phantom on the right and left side. Positions are based on previous intercomparison (Rühm et al., 1998). Figure adapted from Rühm et al. (1998).

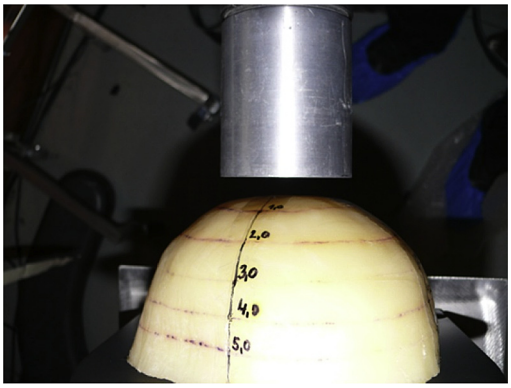

Fig. 5. Measurement position defined for the CSR phantom: side view with detector in measurement position.

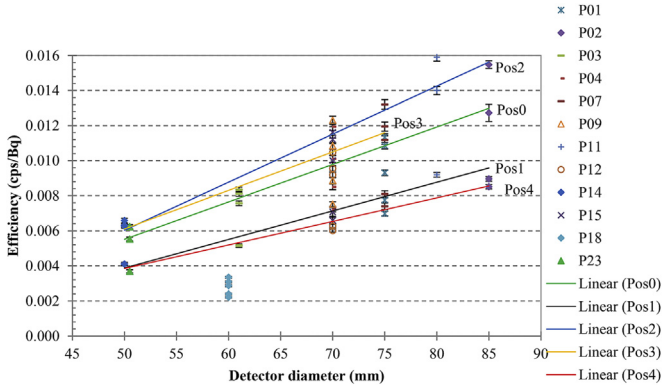

Fig. 6. Results of Task 1–59.54 keV detection efficiency for various positions on the USTUR skull phantom, as a function of PBC detector diameter. Note that the fit does not include the results from P18 and that the one-sigma uncertainty is displayed except when the value is smaller than the symbol.

5.2. Task 2 phantom activity estimation

Six participants delivered results for this task. Each participant was free to use his own calibration phantom and measurement geometry. The phantoms that were used by the participants, for calibrating their PBC systems, are quite different from the intercomparison phantoms. For example, participant P04 used the MCNP 5.1.6 Monte Carlo code and the voxel model "38 year-old

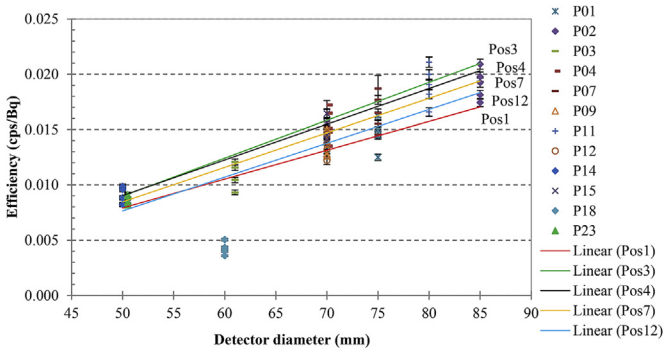

Fig. 7. Results of Task 1–59.54 keV detection efficiency for the BfS skull phantom as a function of PBC detector diameter. Note that the fit does not include the results from P18 and that the one-sigma uncertainty is displayed except when the value is smaller than the symbol.

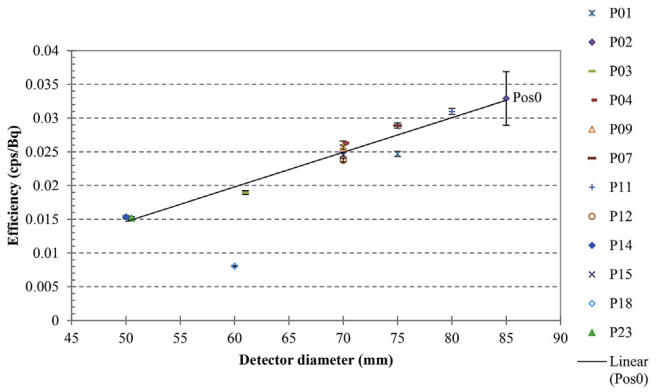

Fig. 8. Results of Task 1–59.54 keV detection efficiency for the CSR phantom as a function of PBC detector diameter. Note that the fit does not include the results from P18 and that the one-sigma uncertainty is displayed except when the value is smaller than the symbol.

woman", which was built based on the CT of a real person (Vrba, 2007), to calibrate their system. In a similar way, participant P07 used the MCNPX 2.6.0 Monte Carlo code and the two voxel phantoms of the ICRP Man and ICRP Woman (ICRP-110B, 2009). In contrast, participant P09 calibrated their PBC system using the UCIN skull phantom, built in 1994 at the University of Cincinnati (Kellar, 1995; Spitz and Lodwick, 2000). Participant P12 calibrated their PBC system using two skull phantoms produced by David P Hickman, at New York University Medical Center, USA (Hickman, 1987/8). Participant P14 used the GEANT4 Monte Carlo code and the MAX-06 voxel phantom, that was built using CT data from the Zubal phantom (Kramer et al., 2006). Finally, participant P15 calibrated their PBC system using the artificial Cohen head phantom, produced by the New York Medical Center, USA (Tables 7 and 8).

In Table 9, one can see that all participants provided reasonable activity estimations for the USTUR Case 0102 skull phantom, the ratio between estimation and real activity varies between 0.77 and 1.52. In contrast, the results obtained for the other phantoms are significantly worse. The BfS phantom activity was overestimated by all participants and the ratio between estimation and real activity varies between factors 1.49 and 3.44.

Because the CSR phantom was developed for the verification of Monte Carlo calculations including voxel phantoms, its geometry is not suitable for the purpose of skull calibration, due to the missing representation of the lower part of the skull bone and mandible bone. The activity estimations shown in Table 9 for the CSR phantom are significantly different from the actual activity, varing between factors 1.90 and 5.69.

5.3. Task 1 result normalization

Because different detectors have different characteristics such as the germanium crystal diameter and thickness, or material and thickness of the end cap, each detector shows unique detection efficiency and is not directly comparable with other detectors. This should be kept in mind when the results obtained by the different participants are compared. In this work a comparison of the results obtained is done by dividing the results of USTUR and BfS phantom by the result of CSR phantom for each participant, so that the detector specific characteristics such as the dead layers thickness, end-cap window material and thickness, and charge collection, which are responsible for the detector intrinsic efficiency, are cancel out. The normalized results for the full energy peak efficiency at 59.54 keV were then compared with the average of the normalized results. In order to estimate the accuracy of the results, the statistical measurement uncertainty was taken into account

Table 7
Task 1 detection efficiency results obtained for the BfS phantom. NP – not provided by the participant. The uncertainty values correspond to the Gaussian uncertainty propagation of the net peak area uncertainty, the gamma emission yield uncertainty and the phantom activity uncertainty.

Position	Participant efficiency and uncertainty (10^{-3}cps/Bq)					
	P01	P02	P03	P04	P07	P09
1	12.5 ± 0.29	17.4 ± 0.38	10.4 ± 0.24	13.5 ± 0.32	14.5 ± 0.33	12.8 ± 0.28
3	14.9 ± 0.34	20.9 ± 0.45	12.1 ± 0.27	17.2 ± 0.40	18.7 ± 1.19	14.0 ± 0.31
4	16.2 ± 0.38	19.8 ± 0.43	12.1 ± 0.27	16.5 ± 0.38	17.7 ± 0.40	14.9 ± 0.33
7	14.5 ± 0.33	19.2 ± 0.41	11.6 ± 0.26	15.1 ± 0.35	16.5 ± 0.37	15.0 ± 0.33
12	14.7 ± 0.33	18.1 ± 0.39	9.31 ± 0.21	14.8 ± 0.35	15.5 ± 0.35	12.6 ± 0.28
	P11	P12	P14	P15	P18	P23
1	16.6 ± 0.39	12.2 ± 0.37	8.20 ± 0.18	14.5 ± 0.35	3.59 ± 0.08	8.18 ± 0.19
3	21.1 ± 0.46	15.3 ± 0.42	9.86 ± 0.22	16.4 ± 0.40	5.05 ± 0.11	9.11 ± 0.21
4	20.0 ± 0.43	14.6 ± 0.41	9.58 ± 0.21	15.6 ± 0.38	4.35 ± 0.09	9.00 ± 0.21
7	19.1 ± 0.41	13.6 ± 0.40	8.82 ± 0.20	15.6 ± 0.38	4.20 ± 0.09	8.50 ± 0.20
12	18.2 ± 0.40	13.2 ± 0.39	8.21 ± 0.18	14.1 ± 0.35	4.01 ± 0.09	8.44 ± 0.19

Table 8
Task 1 detection efficiency results obtained for the CSR phantom. The uncertainty values correspond to the Gaussian uncertainty propagation of the net peak area uncertainty, the gamma emission yield uncertainty and the phantom activity uncertainty.

Position	Participant efficiency and uncertainty (10^{-3}cps/Bq)					
	P01	P02	P03	P04	P07	P09
0	24.7 ± 0.39	32.9 ± 3.97	18.9 ± 0.27	26.3 ± 0.29	28.9 ± 0.39	25.7 ± 0.29
	P11	P12	P14	P15	P18	P23
0	31.0 ± 0.45	23.7 ± 0.27	15.3 ± 0.20	24.6 ± 0.37	8.04 ± 0.10	15.2 ± 0.22

Table 9
EURADOS intercomparison Task 2 results – Total activity estimation for the intercomparison reference date 1 January 2012, calibration phantom used, and ratio to the actual activity in the phantom. NP – not provided by the participant. The actual activities of the intercomparison phantoms at the reference date are: USTUR skull Phantom – 287.2 ± 3.7, BfS – 5239.3 ± 113.4 Bq, CSR – 981.4 ± 9.8 Bq. For details see text.

Participant	Phantom	Activity estimation (Bq)	Uncertainty (Bq)	Calibration phantom	Ratio to real Activity
P04	USTUR	309	30.9	38 year-old woman voxel phantom	1.08
	BfS	7800	780		1.49
	CSR	1860	NP		1.90
P07	USTUR	501	NP	ICRP reference man	1.74
	BfS	18000	NP	ICRP reference woman	3.44
	CSR	NP	NP		–
P09	USTUR	220	11	UCIN skull phantom	0.77
	BfS	7800	400		1.49
	CSR	NP	NP		–
P12	USTUR	339	NP	Two Hickman skull phantoms	1.18
	BfS	9693	NP		1.85
	CSR	NP	NP		–
P14	USTUR	437	52	MAX-06 voxel phantom	1.52
	BfS	15979	1917		3.05
	CSR	5588	670		5.69
P15	USTUR	299.6	NP	Cohen phantom	1.04
	BfS	12702.2	NP		2.42
	CSR	3217.4	NP		3.28

(see Table 1).

Accordingly, in Fig. 9, the relative difference between the normalized USTUR skull phantom results of Task 1 and their average is shown as a function of measurement position (see Fig. 2). The biggest deviation was found for position 1 where the relative difference varies between −14.6% and 13.8%. In contrast, the best agreement was found for position 4, where the relative difference varies between −8.4% and 6.6%. Similarly, for position 0 the relative difference varies between −11.3% and 16.4%, for position 2 it varies between −9.1% and 13.5%, and for position 3 it varies between −8.8% and 9.2%.

For the BfS phantom similar results were observed (see Fig. 10). Here the biggest deviation was found for position 1 where the relative difference varies between −14.4% and 13.1%. In contrast, the best agreement was found for position 4 where the relative difference varies between −11.9% and 6.9%. For position 3 the relative difference varies between −14.0% and 7.7%, for position 7 between −10.3% and 9.2%, and for position 12 between −10.0% and 9.1%.

6. Discussion

The results of Task 1 show that independently of the detector size, the detection efficiency obtained using the USTUR Case 0102 skull phantom depends on the measurement position (see Fig. 6). This is due to several factors:

a) the sagittal division of the skull bone in the phantom;

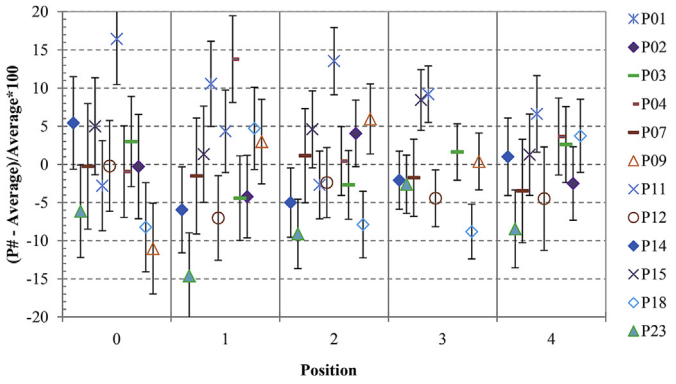

Fig. 9. Relative deviation between the normalized results obtained and their average, for the USTUR Case 0102 skull phantom. All results are normalized with the results obtained using the CSR phantom. Error bars correspond to a one sigma statistical uncertainty. For positions see Fig. 2.

b) the variation of the thickness of the soft tissue equivalent material that covers the skull bone; and
c) the ^{241}Am is not homogenously distributed in the bone surface due to bone remodelling, calcification and resorption.

In contrast, for the BfS phantom the detection efficiency did not depend so much on measurement position (Fig. 7). This is due to the fact that a constant thickness of tissue equivalent wax was used to cover the skull bone, and a homogeneous distribution of the ^{241}Am point sources in the bone surfaces was achieved.

As expected – save for exceptions – the detection efficiency obtained for the 3 phantoms is proportional to the detector diameter. In a few exceptional cases, different intrinsic detector efficiencies which depend on the detector entrance windows and end cap materials and thicknesses, might be the reason. An extreme case is the detector used by P18, because its end cap is completely made of aluminium instead of carbon or beryllium as is the case for the other laboratories (see Table 2); thus, this detector has the lowest efficiency at 59.54 keV.

Due to the proportionality between the detector size and the detection efficiency one can conclude that a bigger detector will have advantages over a small diameter detector, since a small detector will need a longer measurement time to obtain the same counting statistics. For example, the P18 detector due to is aluminium end cap has an efficiency approximately one half of the P14 detection efficiency and one fourth of the P02 detection efficiency, and thus it would need 2 to 4 times longer measurement times to obtain the same counting statistic as P14 and P02 respectively.

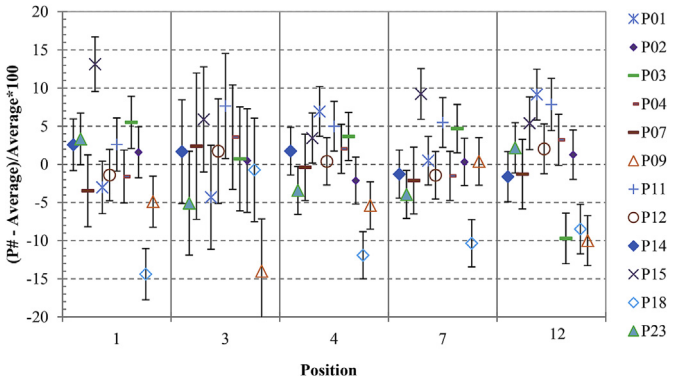

Fig. 10. Relative deviation between the normalised results obtained and their average, for the BfS phantom. All results are normalized with the results obtained using the CSR phantom. Error bars correspond to a one sigma statistical uncertainty. For positions see Fig. 4.

The measurement time is particularly important for *in vivo* measurements, since typically it is not possible to perform long measurements with a living subject, and thus detector with low detection efficiency will have this additional difficulty on the measurement of a low activity radionuclide incorporation.

Normalization of the results with the CSR phantom results allowed comparison of the results obtained by the different PBCs. The relative difference between the participants' results and the average of the results is less than 15% for the BfS phantom and less than 17% for the USTUR skull phantom. Due to the long measurement time required for the measurements, most of the participants were only able to measure each of the measurement positions one time. If the participants had repeated and averaged their measurements, it would be expect that spread observed in Figs. 9 and 10 would decrease, since the averaging of different measurements would reduce the bias due to a different positioning. For *in vivo* routine skull measurements a 13% uncertainty for the positioning of the detectors is generally taken in account (Castellani et al., 2013).

In Task 2, taking into account the variety of different calibration phantoms use by the participants and a typical 13% uncertainty for the positioning of the detectors relative to the phantoms one can conclude that the activity estimates for the USTUR skull phantom were rather good, with a ratio between measured and actual ^{241}Am activity that varies between 0.77 and 1.52. On the other hand, the BfS phantom activity was overestimated by all participants, and the ratio between measured and actual ^{241}Am activity is always above unity and varies between 1.49 and 3.44.

The overestimation observed for the BfS phantom is possibly due to phantom size, since the BfS phantom is very small (possibly the skull bone belonged to a young Asian female) and all participants used Caucasian adult size skull phantoms. Note also that – as demonstrated by Hunt et al. (1999), Vrba (2007), and more recently by Nogueira (2014) – a small size phantom will result in a higher detection efficiency. This effect can result in relative differences of up to 71% between the smallest and the biggest radius of a typical human head size (Nogueira, 2014). The phantom size also explains why the USTUR skull phantom activity estimations are generally better, since this phantom is larger and more similar to the head of an adult Caucasian man.

An additional reason for the discrepancies observed is the soft tissue thickness covering the phantoms' skull bone. As an example the USTUR skull phantom shows a variable scalp thickness that resembles the thickness of a real human scalp, while the BfS phantom shows a constant thickness which represents an average human scalp thickness. On the other hand, voxel phantoms depending on their voxel resolution can have difficulties describing the scalp thickness due to stair step artefacts. Due to these artefacts the voxel phantom skull bone may not completely be covered by the scalp, in the simulations.

The filling of the phantoms can also lead to significant discrepancies. It was emphasized by Vrba (2007) that the brain regions in the USTUR and BfS phantoms are not completely filled, which was discovered on CT images of the phantoms.

Finally, the different ^{241}Am activity distribution present in the phantoms can also contribute to the observed discrepancies: while the voxel phantoms show generally an ^{241}Am activity distribution in the whole volume of the skull bone, in an artificial phantom, such as the BfS, the ^{241}Am activity is typically achieved through the use of small point sources attached to the surface of the skull bone. It was proven that homogenous distribution of the activity on the bone surface gives about 22% higher detection efficiency than the

same skull with homogenous distribution of the activity in the volume (Vrba, 2007). The laboratories which used calibration phantoms with different source distributions than the measured one introduced this bias into their estimates.

Additionally in a real ^{241}Am incorporation, the activity is present both in the cortical and in the trabecular bone and there can be bone remodelling which may result in ^{241}Am activity patterns as those measured by Hickman and Cohen (1988) in the construction of the USTUR skull phantom.

As expected, the activity estimations for the CSR phantom are less accurate. All participants overestimated the actual ^{241}Am activity by a factor of 1.9–5.69. In this case, the overestimation observed is mainly due to this phantom representing only the top part of the skull and, consequently, the efficiency of the measurement is greater than that of the whole skull calibration phantom, thus causing an overestimation of the activity of the CSR phantom.

Taking into account better agreement between the Task 2 activity estimations and the real phantom activity, the superior detail on the scalp thickness description and the size of the phantom being more similar to the average Caucasian adult male, it can be assumed that in general the USTUR Case 0102 skull phantom provides better results than the BfS skull phantom. However, this phantom as several drawbacks such as the activity distribution pattern in the bone surface that can bias the efficiency calibration results; the missing contribution to the count rate due to the use of non-contaminated bone in the fabrication of the phantom; and the incomplete filling of the brain region. Due to these drawbacks it is concluded that none of the intercomparison phantoms is fully adequate for the calibration of a PBC without the use of correction factors to address the phantoms inaccuracy, in describing human anatomy and that as future work a new reference “skull phantom” and the respective voxel model should be fabricated.

7. Conclusions

Due to the small number of skull calibration phantoms for ^{241}Am, only a limited number of laboratories have calibrate their PBC systems for skull measurement geometries, prior to this intercomparison. As a result of the WG7 EURADOS action described in the present paper, now 12 laboratories in Europe and North America have their PBC calibrated for this geometry.

The CSR phantom previously used in the verification of Monte Carlo simulation and voxel models was used in this work for normalization of the Task 1 results. Thanks to this approach it was possible to demonstrate that in general an excellent agreement was found between the results obtained by the participants of the EURADOS exercise, with relative deviations of less than 15% for the BfS phantom and of less than 17% for the USTUR skull phantom. However, for Task 2 the results obtained for the estimation of the phantoms' ^{241}Am activity show significant discrepancies from the default values of up to a factor of 3.4. This is due to the differences between the calibration phantom and the intercomparison phantoms, in terms of skull size, scalp thickness, skull filling and ^{241}Am activity distribution.

In addition to the experience gained, this intercomparison also revealed some of the difficulties associated with the use of the USTUR and BfS skull phantoms and emphasized the need for the fabrication of a ”reference skull phantom” and the respective voxel model. This new reference phantom would allow future activity estimations performed by different laboratories to be more precise. However, to increase the activity estimation accuracy this “reference skull phantom” requires a great level of detail on the reproduction of the geometrical and physical characteristics of the human head. Ultimately the new phantom voxel model together with Monte Carlo methods could then be used to calculate correction factors which would allow calibration of a PBC for individual specific characteristics. This, so called, Person specific calibration has been recently demonstrated to improve the efficiency calibration by up to a factor 1.9 (Nogueira, 2014).

As future work, a similar study performed with Whole Body Counter (WBC) detectors could be of interest. However, since a typical WBC is focussed on energies above 100 keV, most WBC detectors possess low detection efficiencies for ^{241}Am; additionally typical WBC detectors are mounted in fixed structures that reduce the positioning freedom required for skull measurements. Thus for the majority of WBCs the practical implementation of a skull counting geometry will be limited.

Acknowledgments

This study was supported by the German Federal Ministry of Education and Research (Contract No. 02NUK015B) and by the European Radiation Dosimetry Group. The content of the report is solely the responsibility of the authors.

The USTUR is funded by U.S. Department of Energy, Office of Domestic and International Studies (AU-13), under Grant Award No DE-HS0000073.

References

Breitenstein, B.D., Newton, C.E., Norris, H.T., Heid, K.R., Robinson, B., Palmer, H.E., Rieksts, G.A., Spitz, H.B., McInroy, J.F., Boyd, H.A., Eutsler, B.C., Romero, D., Durbin, P.W., Schmidt, C.T., 1985. The U.S. transuranium registry report on the Am-241 content of a whole body. Health Phys. 49, 559–648.

Castellani, C.M., Marsh, J.W., Hurtgen, C., Blanchardon, E., Berard, P., Giussani, A., Lopez, M.A., 2013. IDEAS Guidelines (Version 2) for the Estimation of Committed Doses from Incorporation Monitoring Data. European Radiation Dosimetry e.

Ferreux, M.C.L.J.P.L., 2008. Measurement of 241Am L X-ray emission probabilities. Appl. Radiat. Isotopes 66, 715–721.

Hickman, D.P., 1987/8. Thesis, New York University Medical Center/Institute of Environmental Medicine New York University Medical Center.

Hickman, D.P., Cohen, N., 1988. Reconstruction of a human skull calibration phantom using bone sections from an 241Am exposure case. Health Phys. 55, 59–65.

Hunt, J.G., Malátová, I., Foltánová, S., 1999. Calculation and measurement of calibration factors for bone-surface seeking low energy gamma emitters and determination of 241Am activity in a real case of internal contamination. Radiat. Prot. Dosim. 82, 215–218.

ICRP-78, 1997. Individual Monitoring for Internal Exposure of Workers. In: ICRP Publication 78. Pergamon Press, Oxford, UK.

ICRP-110B, 2009. Adult Reference Computational Phantoms. In: ICRP Publication 110 39, pp. 3–5.

Kellar, J., 1995. Fabrication of an Anthropomorphic Calibration Phantom for in Vivo Measurement of 152Eu in the Skull, Department of Mechanical, Industrial and Nuclear Engineering. University of Cincinnati, Cincinnati, Ohio.

Kramer, R., Khoury, H.J., Vieira, J.W., Lima, V.J., 2006. MAX06 and FAX06: update of two adult human phantoms for radiation protection dosimetry. Phys. Med. Biol. 51, 3331–3346.

Laurer, G., 1993. Letter to W. Burkhart from 8th April 1993. New York University Medical Center. Laboratory for Radiation Studies.

Lopez, M.A., Balásházy, I., Bérard, P., Blanchardon, E., Breustedt, B., Broggio, D., Castellani, C.M., Franck, D., Giussani, A., Hurtgen, C., James, A.C., Klein, W., Kramer, G.H., Li, W.B., Marsh, J.W., Malatova, I., Nosske, D., Oeh, U., Pan, G., Puncher, M., Teixoto Telles, P., Schimmelpfeng, J., Vrba, T., 2011. EURADOS coordinated action on research, quality assurance and training of internal dose assessments. Radiat. Prot. Dosim. 144, 349–352.

Lopez, M.A., Nogueira, P., 2012. EURADOS – internal dosimetry network. In: Parker, M.D., Tolmachev, S.Y. (Eds.), Annual Report FY2011/2012. US Transuranium and Uranium Registries, Washington State University, Richland. WA.

McInroy, J.F., Boyd, H.A., Eutsler, B.C., Romero, D., 1985. The U.S. transuranium registry report of the 241Am content of a whole body. Part IV: preparation and analysis of the tissues and bones. Health Phys. 49, 587–621.

Nogueira, P., 2014. Person-specific Calibration of a Partial Body Counter. Faculty of Medicine. Ludwig-Maximiliabs University München, p. 154.

Rühm, W., König, K., Malátová, I., Doerfel, H., Foltanova, S., Sahre, P., Schütz, R., Wahl, W., 1998. Intercomparison exercise for the determination of Am-241 in the human skeleton. Radiat. Prot. Dosim. 79, 517–521.

Spitz, H.B., Lodwick, J., 2000. Design, fabrication & evaluation of a new calibration phantom for in vivo measurement of bone-seeking radionuclides. Radiat. Prot. Dosim. 89, 275–282.

Tolmachev, S., 2012. United States Transuranium and Uranium Registries (personal communication).

Vrba, T., 2007. Development and application of anthropomorphic voxel phantom of the head for in vivo measurement. Radiat. Prot. Dosim. 127, 201–204.
Vrba, T., 2010. Comparison of geometries for in vivo measurements of actinides in the skull. Appl. Radiat. Isotopes 68, 918–921.
Vrba, T., Broggio, D., Caldeira, M., Capello, K., Fantínová, K., Franck, D., Gómez-Ros, J.M., Hunt, J., Kinase, S., Leone, D., Lombardo, P.A., Manohari, M., Marzocchi, O., Moraleda, M., Nogueira, P., Ośko, J., Arron, S., Suhl, S., Takahashi, M., Teles, P., Tremblay, M., Tymińska, K., Lopez, M.A., Tanner, R., 2015. EURADOS intercomparison exercise on MC modelling for the in-vivo monitoring of AM-241 in skull phantoms (Part II and III). Radiat. Phys. Chem. 113, 59–71.
Vrba, T., Malátová, I., Fojtík, P., Fülöp, M., Ragan, P., 2014a. A simple physical phantom for an intercomparison exercise on Am-241 activity determination in the skull. Radiat. Prot. Dosim. 158, 224–229.
Vrba, T., Nogueira, P., Broggio, D., Caldeira, M., Capello, K., Fantínová, K., Figueira, C., Hunt, J., Leone, D., Murugan, M., Marzocchi, O., Moraleda, M., Shutt, A., Suh, S., Takahashi, M., Tymińska, K., Antonia Lopez, M., Tanner, R., 2014b. EURADOS intercomparison exercise on MC modeling for the in-vivo monitoring of Am-241 in skull phantoms (Part I). Radiat. Phys. Chem. 104, 332–338.